FY2020 FES Theory Milestone

"Modeling of Fully 3D Vertical Displacement Event Disruptions"

Third quarterly Progress Report – June 30 2020

Prepared by: S.C. Jardin, *PPPL*, **C. R. Sovinec,** *U. Wisconsin-Madison*

Summary: The proposed third quarter FY20 milestone was: "Perform and document benchmark M3D-C1/NIMROD 3D VDE calculations in simplified geometry". This has been accomplished and is described in the following pages. A third code, JOREK, also participated in the benchmark.

1. Introduction

The first-quarter FY20 progress report described a 2D vertical displacement event (VDE) benchmark activity involving the 3D MHD codes NIMROD [1], M3D-C1 [2,3] and also the European code JOREK [4]. This study has now been published [5]. The three codes involved in that and in this present study are each fully 3D MHD codes that include a plasma region, a resistive wall, and an outer vacuum region exterior to the wall. However, for the first-quarter benchmark the three codes were constrained to be 2D (axisymmetric). These 2D studies are useful for describing VDEs because experimentally, the plasma is observed to remain axisymmetric for most of the event, and other 2D codes have been successful in reproducing many aspects of the VDE, including the amount of halo current produced and the net vertical force on the vessel [6, 7]. Running in 2D is also much less computationally demanding than running the codes in their fully 3D mode.

However, all VDEs terminate in a 3D unstable state and there are many aspects of a VDE that can only be described by a 3D code. Among these is the horizontal or "sideways" force that has been measured to be substantial in JET [8] and is a concern for ITER [9]. There have been 3D calculations of VDEs published [10, 11] that appear to be in qualitative agreement with some experimental results, but they have not been rigorously validated against experimental data. In addition, no two codes have tried to model the same experimental discharge to see to what degree they agree. Because these sideways forces are a concern for ITER, it is imperative that 3D MHD codes being used to calculate these forces be verified through benchmarking exercises as well as be validated by comparison with existing data.

This report describes such a 3D VDE code benchmarking activity, the first of its kind. In Section 2 we describe the problem setup, Section 3 describes the results, and we summarize and discuss future directions in Section 4.

2. Problem Setup

In order to take maximum advantage of the previous 2D benchmark, we use the same initial geometry and plasma equilibrium as described in the Q-1 milestone report [5]. This was based on NSTX discharge #139536 at 309 ms at which time the vertical feedback system was disengaged and the plasma column became VDE unstable. Instead of trying to model the actual NSTX vacuum vessel, the benchmark

calculations used a simplified nearly rectangular wall shape that all codes could handle. The transport and other dissipation coefficients used in the 2D and 3D benchmark cases are described in Table 1.

Coefficient	Publ. 2D case pre LCFS contact	Publ. 2D case post LCFS contact	New 2D pre LCFS contact	3D post LCFS contact
η_0 (Ohm-m)	3.12×10^{-5}	3.12×10^{-5}	3.12×10^{-4}	3.12×10^{-4}
η_w (Ohm-m)	3×10^{-6}	3×10^{-6}	3×10^{-5}	3×10^{-5}
D (m^2/s)	0.154	30.8	1.54	40.
$\kappa_\perp$ (1/m·s)	1.54×10^{18}	7.70×10^{20}	1.54×10^{19}	1.54×10^{21}
$\kappa_{\|\|}$ (1/m·s)	1.54×10^{23}	1.54×10^{23}	1.54×10^{24}	1.54×10^{26}
ν (kg/m·s)	5.16×10^{-7}	5.16×10^{-7}	5.16×10^{-7}	5.16×10^{-7}

Table 1: Transport and other dissipation coefficients used in 2D and 3D benchmarks. Spitzer resistivity was used with η_0 being the value associated with 15 eV, η_w is the wall resistivity, D the particle diffusion, $\kappa_\perp$ and $\kappa_{||}$ the isotropic and parallel thermal conductivities, and ν the viscosity. LCFS contact is when the plasma switches from being diverted to being limited by the vessel.

A Spitzer-like resistivity was used with $\eta(T) = \eta_0(T_0/T)^{3/2}$, T_0 = 15 eV. The Alfven time for the original equilibrium was $\tau_A \cong 1$ μs and the L/R time for the vessel used in the 3D calculations was 0.15 ms.

The NIMROD calculation used ~39,000 bi-cubic elements interior to the vacuum vessel. Runs were made both with $0 \le n \le 10$ and with $0 \le n \le 21$ toroidal harmonics. For accuracy with NIMROD's implicit leapfrog, the flow-CFL number was not allowed to exceed unity. The net force on the resistive wall was calculated as a surface integral over the outer wall surface, $F_j = \mu_0^{-1} \oint d\mathbf{S} \cdot \left[\mathbf{BB} - \mathbf{I}B^2/2 \right] \cdot \hat{\mathbf{e}}_j$ [12]. At 9.4 ms (1.1 ms into the 3D phase) a parallel viscosity $\nu_{||} = 100\,\nu$ was introduced to avoid mesh scale noise on the tokamak's outboard side.

The M3D-C1 calculation used the unstructured poloidal plane mesh shown in Figure 1, which has 17,424 vertices on each plane, each with 12 DOF for each scalar field in 3D (6 in 2D). The 3D phase used 16 toroidal Hermite cubic finite elements for each of the triangular vertices. A normalized time step of dt=0.5 τ_A was used, except for a period of .048 ms, starting at time 10.185 ms (1.233 after the start of the 3D) when it was halved to dt=0.25 τ_A, to avoid numerical instability. After this time, a "upwind" second order toroidal diffusion term was added to the scalar convection terms for the pressure, density, and magnetic field, equal to 0.05 Vφ. The wall force in M3D-C1 is calculated by integrating $\int \mathbf{J} \times \mathbf{B} dV$ over all the elements within the vessel.

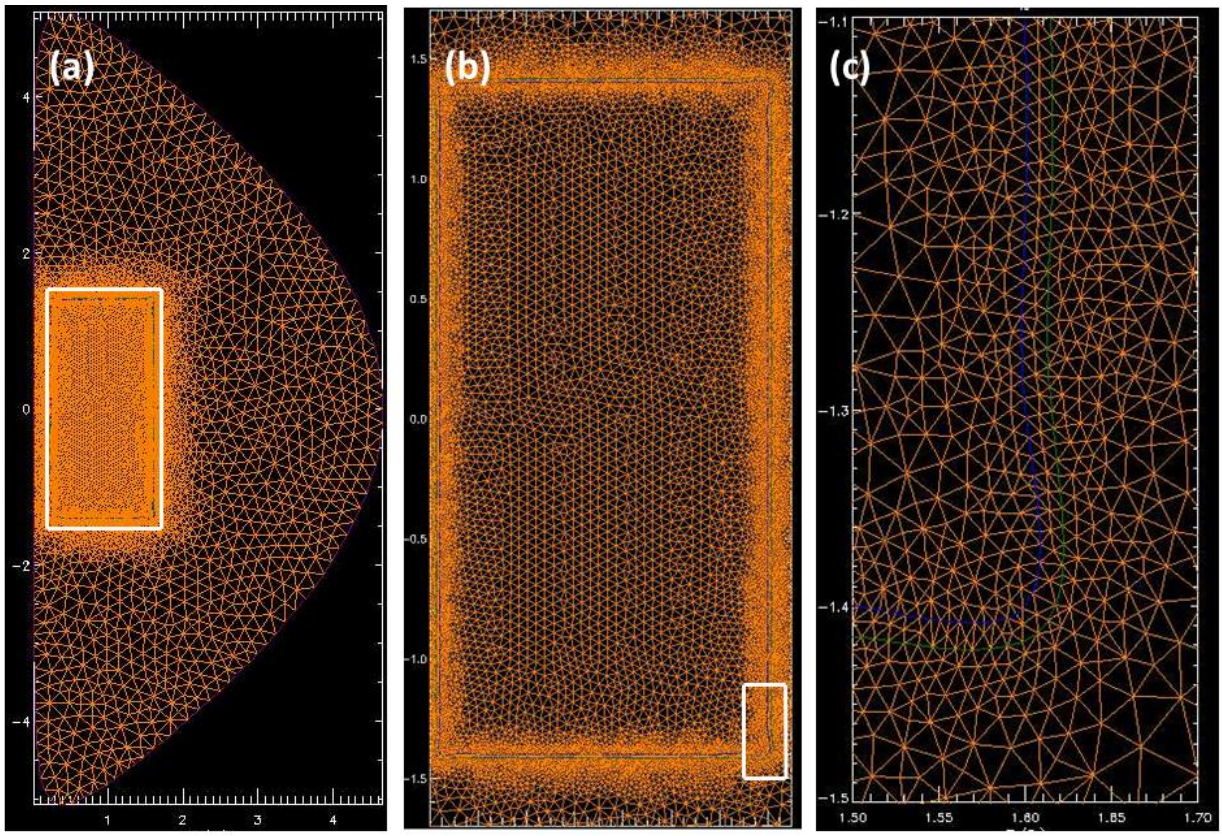

Figure 1: Poloidal unstructured mesh used in M3D-C1 calculation. White rectangles in (a) and (b) are blown-up in (b) and (c)

3. Computational Results

As described in Section 2, the calculations began in 2D with an axisymmetric plasma drifting downward due to the vertical instability. Once the separatrix, or last closed flux surface (LCFS), made contact with the vessel wall, the calculation was switched to 3D and continued. The 2D phase has been described in the Q1 report and in Ref. [5] (although with slightly different dissipation parameters as detailed in Table 1) so here we concentrate on the 3D segment.

Figure 2 summarizes some of the 0D, scalar, results of the three codes during the 3D phase. Figures (2a) and (2b) are the Z and R positions of the magnetic axis. Note that towards the end of the calculation, when all the flux surfaces have been destroyed, there is no well-defined position of the magnetic axis and the different codes make approximations that are not identical for this diagnostic. Figure (2c) plots the plasma current within the LCFS (solid line) and within the vacuum vessel (dotted line). Note that since NIMROD does not compute a magnetic flux function, it only outputs the current inside the vacuum vessel. The plasma current diagnostics for within the LCFS for M3D-C1 and JOREK differ towards the end as the surfaces become stochastic and the LCFS is not well defined.

Figure (2d) is the thermal energy within the plasma during the 3D phase of the calculation. All three codes see a pronounced drop at about 1.0 ms after the start of the 3D phase. This is due to parallel transport in the now stochastic field lines. Figure (2e) shows the number of particles within the LCFS in

JOREK and M3D-C1. There is a constant offset, the origin of which is being looked into, but they show the same trends. Figure (2f) shows the measure of internal inductance known as li(3) for the JOREK and M3D-C1 calculation. Here, $\ell_i(3) \equiv 2B_p^2 \Big/ \left(\mu_0 I_p^2 R_0 \right)$. Again, there is generally good agreement until the surfaces break up and the LCFS is ill-defined.

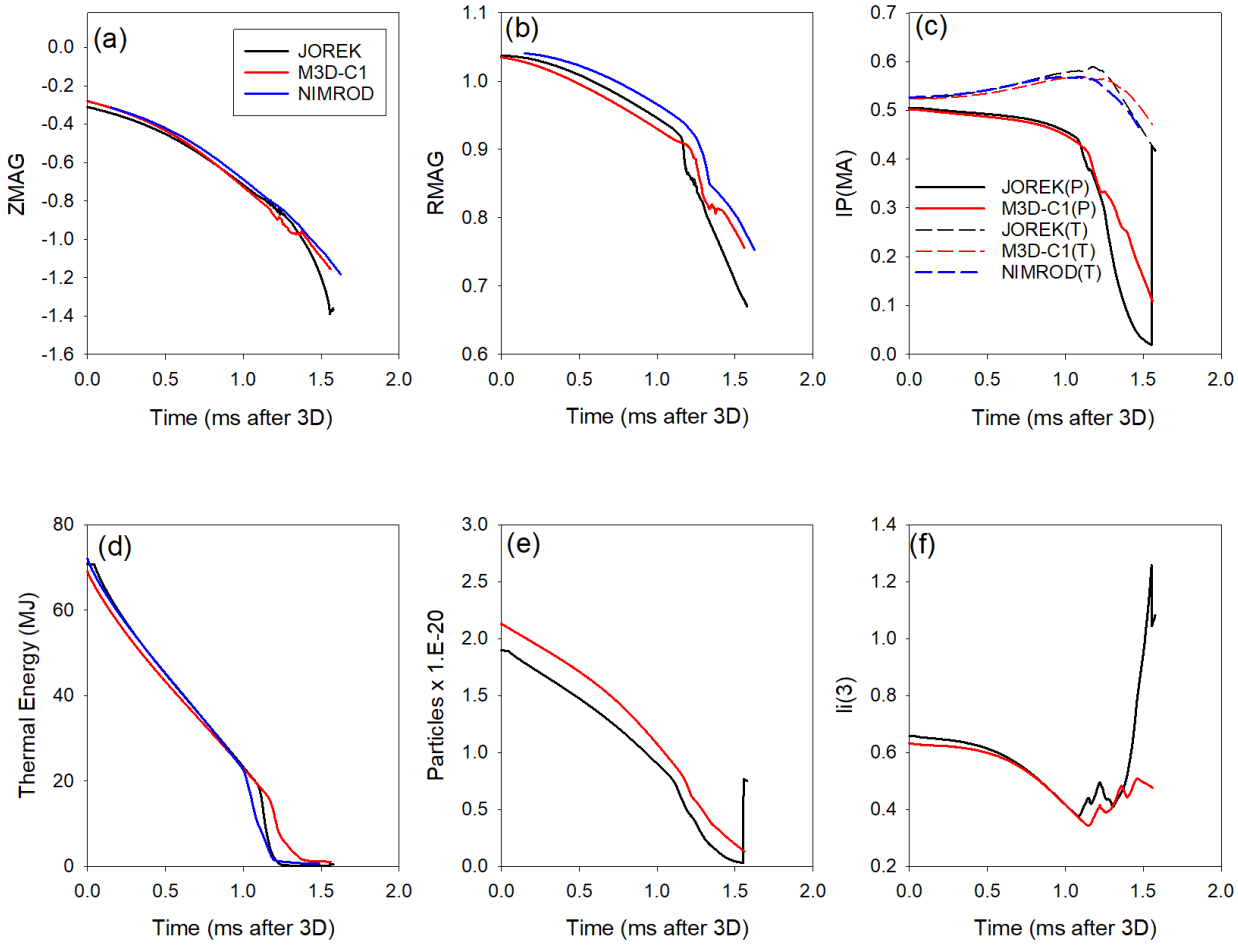

Figure 2: Comparison of 0D quantities during the 3D phase of the calculation. (a,b) the z and R position of the magnetic axis, (c) the toroidal current within the LCFS (solid) and within the vessel (dashed), (d) the thermal energy within the plasma, (e) the number of particles within the LCFS, and (f) the internal inductance li(3).

Figure 3 shows the magnetic energy in the first 5 Fourier harmonics for the 3 codes. The results from the 3 codes are not identical, but they are qualitatively very similar. All codes show that the n=1 harmonic (red line) has the largest amplitude throughout the calculation, although the n=2 and n=3 harmonics approach it during the strong growth phase that occurs about 1 ms after the start of the 3D calculation. The fact that the energy in the higher harmonics (n=4,5) remain smaller than that in the lower harmonics (n=1,2,3) indicate that the calculations are adequately resolved in the toroidal direction.

In Figures 4 and 5 we plot contours of the pressure at the φ=0 plane at three times over the span of 0.1 ms as the thermal quench (TQ) is occurring for both the NIMROD and M3D-C1 calculations. It is seen

that there is complex MHD activity occurring that destroys the outer flux surfaces. Note that the times listed are offset from each other by about 0.8 ms, which we can attribute to differences in the time the two 3D calculations started due to differing initial 2D VDE displacements.

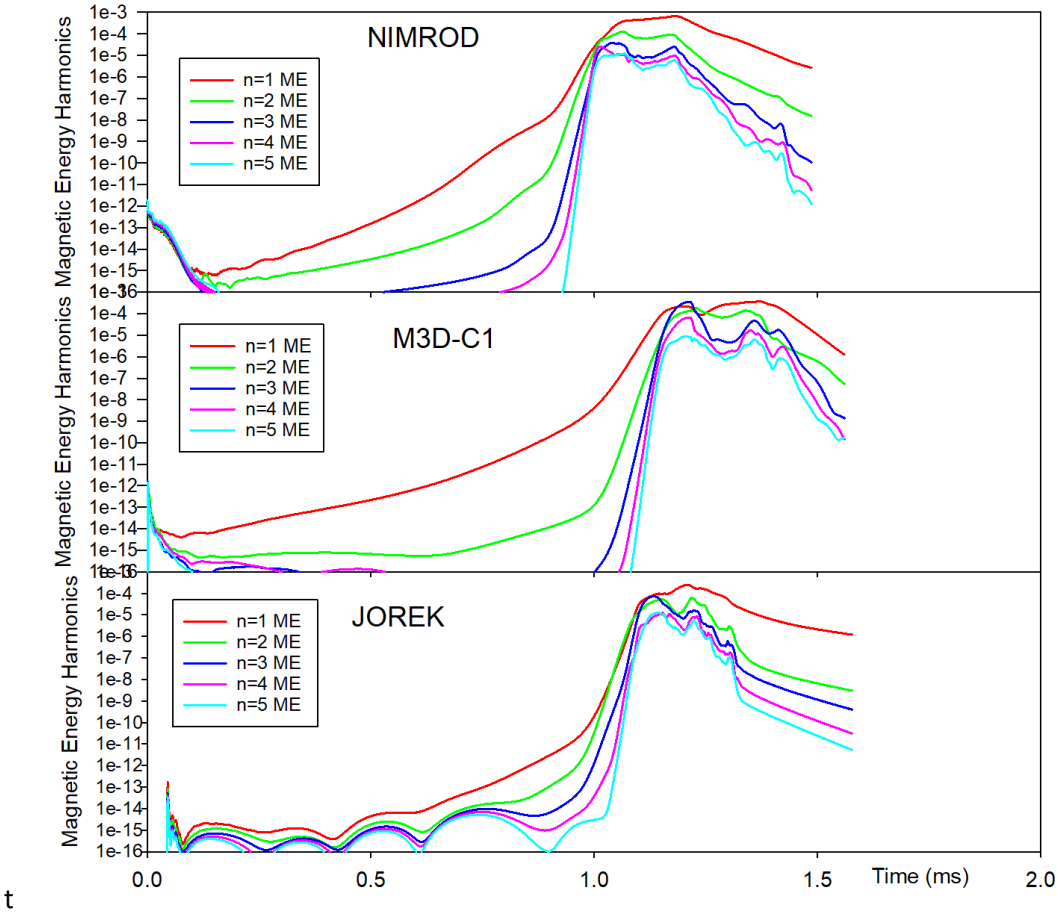

t

Figure 3: Magnetic energy in the different Fourier harmonics as a function of time for the 3 codes.

In Figure 6, we plot the growth rates for the first 8 harmonics, defined as $\gamma_n \equiv \dot{E}_n / E_n$ where E_n is the magnetic energy in the nth toroidal harmonic, the first 5 of which are plotted in Fig. 3. The bottom row is a close-up of the time around 1 ms after the start of the 3D calculation, when both the amplitudes of the harmonics and their growth rates are at a maximum. While the details differ, all codes show a similar trend. The first mode with a significant growth rate is the n=1 mode, plotted as a red line. That then drives the n=2 mode which obtains a growth rate approximately double that of the n=1 mode. The n=1 and n=2 modes combine to drive the n=3 mode at about 3 times the growth rate of the n=1 mode. This trend continues for all modes shown, and so the n=8 mode has the highest growth rate even though it has the lowest amplitude.

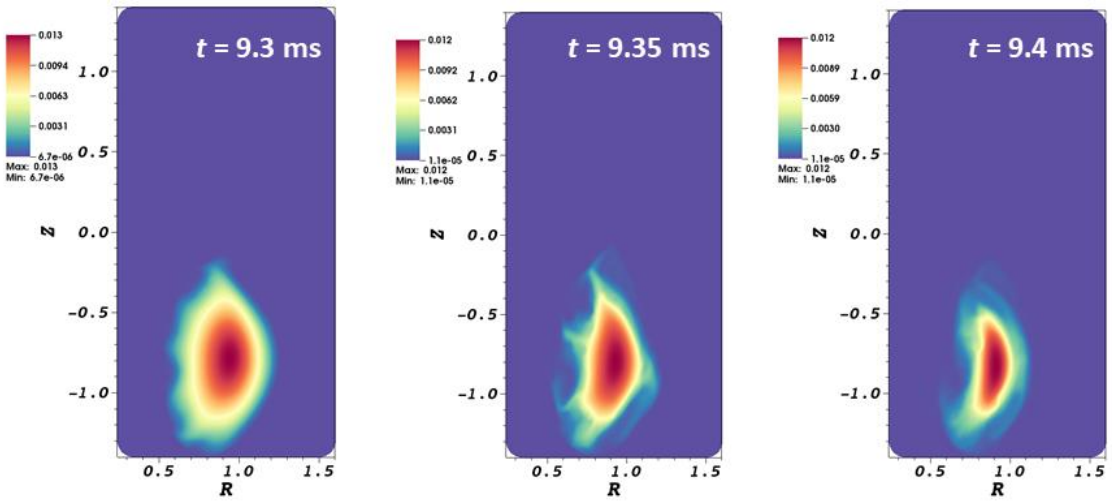

Figure 4: Contour plots of the pressure (dimensionless units) at three times around the main thermal quench. Shown is pressure on the φ=0 plane for the 0 ≤n≤ 21 computation. Times are relative to the start of the initial 2D calculation.

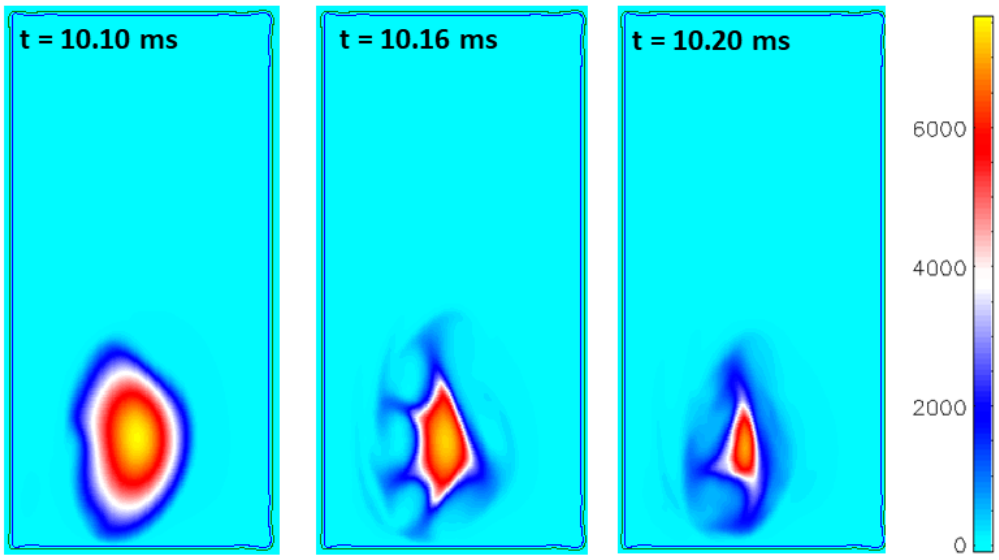

Figure 5: Contour plots of pressure (SI units) at the φ=0 plane at three times around the main thermal quench for the M3D-C1 calculation. Times are relative to the start of the initial 2D calculation.

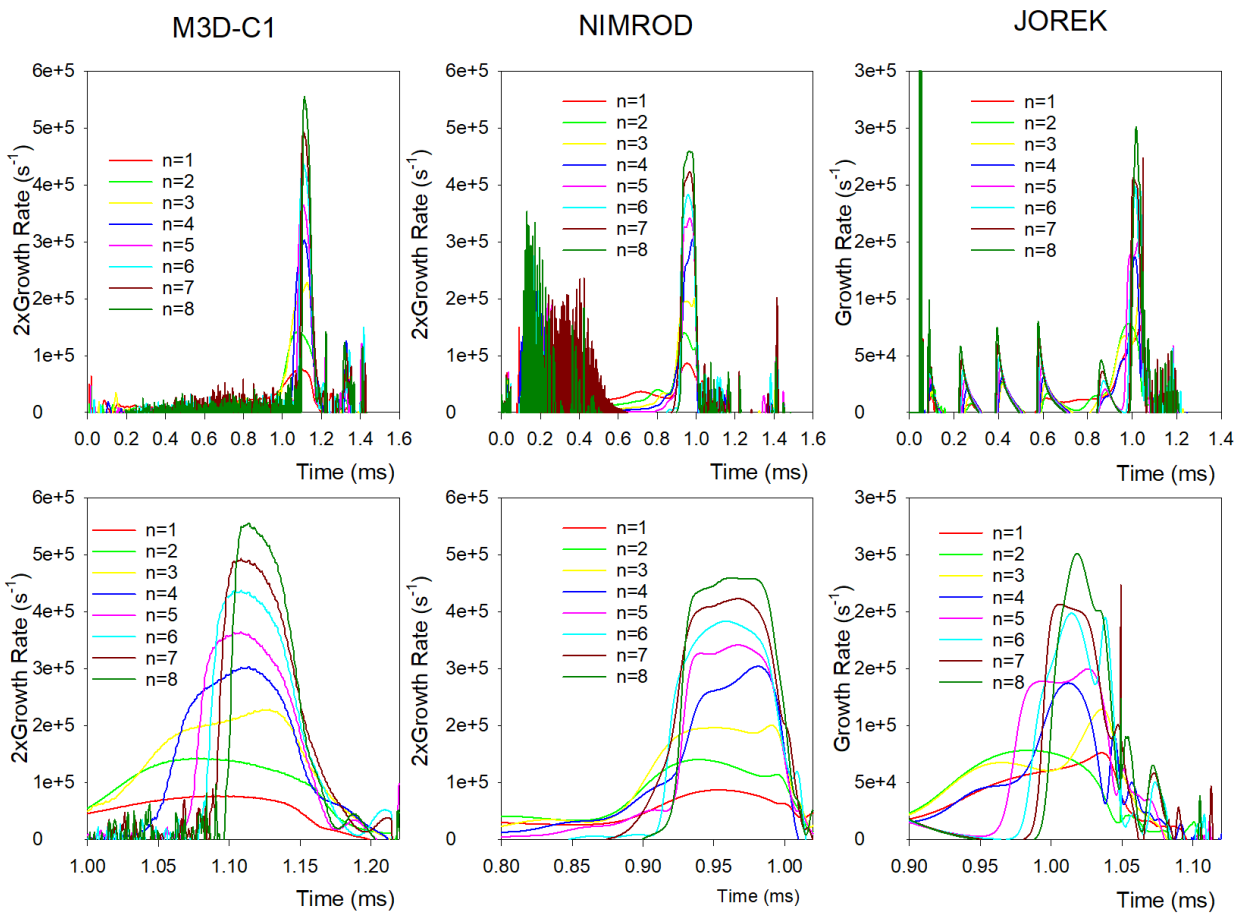

Figure 6: Growth rates in the different magnetic energy harmonics shown in Figure 3 The bottom row is a close-up of the period around 1.0 ms when the energies and their growth rates peak.

The primary result of these calculations is the forces that occur on the vacuum vessel as a result of the violent MHD activity. A force diagnostic for the JOREK code is presently under development, so only the forces calculated by NIMROD and M3D-C1 are shown in Figure 7. There are two forces that are of primary interest, the vertical force and the horizontal force, sometimes known as the sideways force. The vertical force is primarily caused by the n=0 axisymmetric motion of the plasma column and by the current quench, so it can be determined to a large degree by a 2D (axisymmetric simulation) but the horizontal force is a fundamentally 3D phenomena that arises primarily from the n=1 component of the magnetic field and current. In Figure 7 we see there is very good agreement between the two codes for each of these forces. (Note we have time-shifted the results so that the increase in the horizontal forces begin at the same times.) The magnitudes of the two forces are very similar. The fact that the M3D-C1 result for the n=1 horizontal force is more "noisy" than the NIMROD result is likely due to the fact that, as explained in Section 2, the M3D-C1 diagnostic integrates the $\mathbf{J}\times\mathbf{B}$ force directly over the vessel elements, whereas the NIMROD code evaluates the force from the field outside the vessel, likely causing a smoothing effect. This is being looked into further.

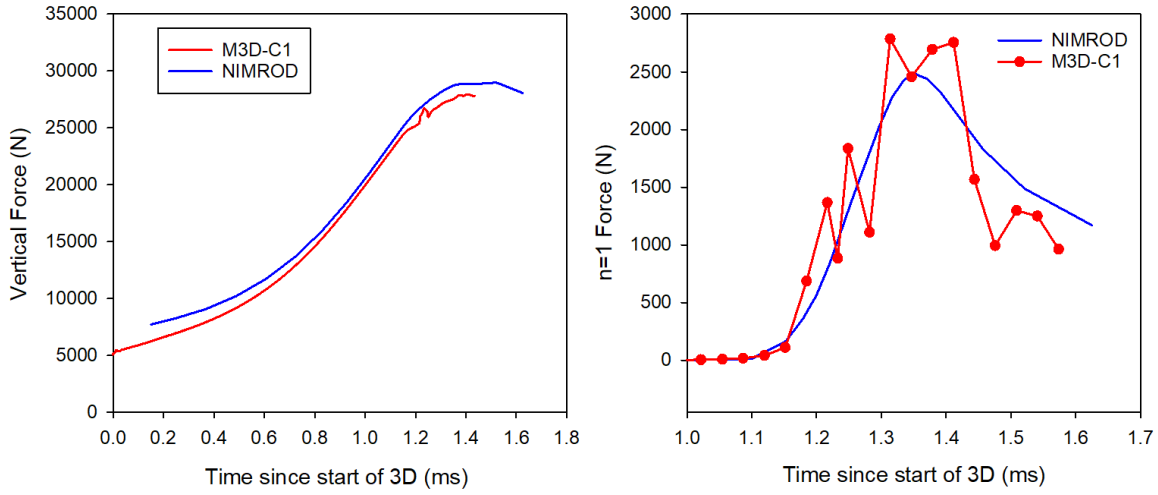

Figure 7 Forces in the vertical and horizontal directions as calculated by NIMROD and M3D-C1

4. Summary and Future Directions

We carried out a 3-code benchmarking activity in which the NIMROD, M3D-C1, and JOREK codes were applied to the same problem: a fully 3D simulation of a vertical displacement event. The codes were initialized with the same geqdsk equilibrium, implemented the same geometry of the conducting vacuum vessel, and used the same dissipation coefficients. Each code began the calculation in 2D, and continued the solution in 3D once the plasma column made contact with the vessel. The results of the 3 codes are in good qualitative agreement with respect to the 0D quantities compared (for example, plasma current and stored energy vs time) as well as the energies in the different Fourier harmonics. The growth rates of the different Fourier harmonics all show a similar structure with the n=1 being the dominant instability, which drives the higher-n modes at multiples of its growth rate. The peak forces on the vacuum vessel as calculated by NIMROD and M3D-C1 differ by about 3% for the vertical force and 15% for the sideways force. Efforts are underway to understand the origins of these differences, and also to calculate and compare additional diagnostics such as the toroidal peaking factor of the halo current.

Acknowledgements

The calculations documented here were carried out by S. Jardin(PPPL), C. Sovinec (University of Wisconsin-Madison), F. J. Artola (ITER Organization), M. Hoelzl (Max Plank Institute for Plasma Physics), N. Ferraro, C. Clauser (PPPL) and I. Krebs(FOM Institute DIFFER – Dutch Institute for Fundamental Energy Research) This work was supported by US DOE Contracts No. DE-AC02-09CH11466 and No. DE-SC0018001, and the SciDAC Center for Tokamak Transient Simulations. Some of the computations presented in this report used resources of the National Energy Research Scientific Computing Center (NERSC), a U.S. Department of Energy Office of Science User Facility operated under Contract No. DE-AC02-05CH11231. The support from the EUROfusion Researcher Fellowship

programme under the task agreement WP19-20-ERG-DIFFER/Krebs is gratefully acknowledged. Part of this work has been carried out within the framework of the EUROfusion Consortium and has received funding from the Euratom research and training programme 2014-2018 and 2019-2020 under grant agreement No 633053. The views and opinions expressed herein do not necessarily reflect those of the European Commission.

References

[1] C. R. Sovinec, A. H. Glasser, T. A. Gianakon, D. C. Barnes, R. A. Nebel, S. E. Kruger, D. D. Schnack, S. J. Plimpton, A. Tarditi, M. S. Chu, and the NIMROD Team, "Nonlinear magnetohydrodynamics simulation using high-order finite elements," *Journal of Computational Physics*, **195,** pp. 355–386, (2004).

[2] S. C. Jardin, N. Ferraro, J. Breslau, and J. Chen, "Multiple timescale calculations of sawteeth and other global macroscopic dynamics of tokamak plasmas," *Computational Science & Discovery*, **5**, 014002, (2012)

[3] N. M. Ferraro, S. C. Jardin, L. L. Lao, M. S. Shephard, and F. Zhang, "Multi-region approach to free-boundary three-dimensional tokamak equilibria and resistive wall instabilities," *Physics of Plasmas*, **23**, 056114, (2016).

[4] G. Huysmans and O. Czarny, "MHD stability in x-point geometry: simulation of ELMs," *Nuclear fusion*, **47**, p. 659, (2007).

[5] I. Krebs, F. J. Artola, C. R. Sovinec, S. C. Jardin, K. J. Bunkers, M. Hoelzl, and N. M. Ferraro, "Axisymmetric simulations of vertical displacement events in tokamaks: A benchmark of M3D0C1, NIMROD, and JOREK", *Phys. Plasmas* **27**, 022505, (2020)

[6] R. Sayer, Y. Peng, S. Jardin, A. Kellman and J. Wesley et al, "TSC Plasma Halo Simulation of a DIII-D Vertical Displacement Episode", *Nuclear Fusion* **33** p. 969-978 (1993)

[7] J. Lee and J. Kim, "Simulation study of the disruption load in KSTAR device with a modified passive stabilizer", *Journal of the Korean Physical Society* **64** 396-404 (2014)

[8] V. Riccardo, P. Noll, S. Walker, "Forces between plasma, vessel and TF coils during AVDEs at JET", *Nuclear Fusion* **40** 1805 (2000)

[9] M. Lehnen, K. Aleynikova, P. Aleynikov, D. Campbell, P. Drewelow, N. Eidietis, Y. Gasparyan, R. Granetz, Y. Gribov, N. Hartmann, et al, "Disruptions in ITER and strategies for their control and mitigation*", Journal of Nuclear Materials***, 463** 39-48 (2015)

[10] H. Strauss, "Comparison of JET AVDE disruption data with M3D simulations and implications for ITER", *Phys. Plasmas* **24**, 102512 (2017)

[11] D. Pfefferlé, N. Ferraro, S. C. Jardin, I. Krebs, and A. Bhattacharjee, "Modelling of NSTX hot vertical displacement events using M3D-C1," *Physics of Plasmas*,. **25**, 056106, 2018

[12] V. D. Pustovitov, “General approach to the problem of disruption forces in tokamaks” *Nucl. Fusion* **55,** 113032 (2015)